Advanced bi-functional CoPi co-catalysts decorated g-C_3N_4 nanosheets coupled with ZnO nanorods arrays as integrated photoanodes

Chang Liu [a], Pengcheng Wu [a], Keliang Wu [a], Guihua Meng [a], Jianning Wu [a], Juan Hou [a,b,*], Zhiyong Liu [a,*], Xuhong Guo [a,c]

[a] School of Chemistry and Chemical Engineering, Shihezi University/Key Laboratory for Green Processing of Chemical Engineering of Xinjiang Bingtuan/Key Laboratory of Materials-Oriented Chemical Engineering of Xinjiang Uygur Autonomous Region/Engineering Research Center of Materials-Oriented Chemical Engineering of Xinjiang Bingtuan, Shihezi, Xinjiang 832003, PR China

[b] College of Science/Key Laboratory of Ecophysics and Department of Physics of Xinjiang Bingtuan, Shihezi 832003, Xinjiang, P. R. China.

[c] State Key Laboratory of Chemical Engineering, East China University of Science and Technology, Shanghai 200237, P. R. China.

∗ Corresponding author: Zhiyong Liu, Ph.D. Juan Hou, Ph.D.

School of Chemistry and Chemical Engineering/Key Laboratory for Green Processing of Chemical

Engineering of Xinjiang Bingtuan, Xinjiang, P. R. China., 832003

Address: Beisi Road, Shihezi City, Xinjiang, 832003, P. R. China.

Tel: 0086-0993-2057276,

E-mail Address: lzyongclin@sina.com,

E-mail Address: hjuan05@sina.com

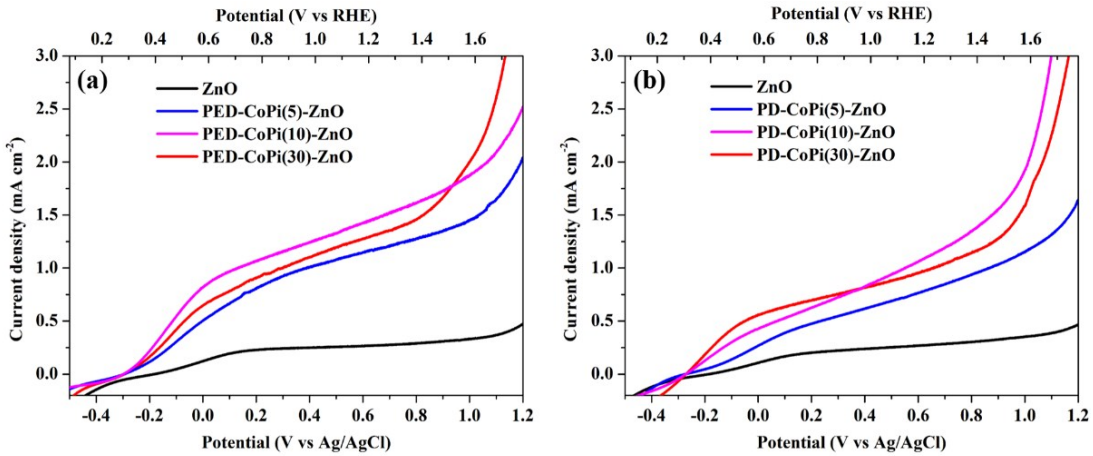

Fig. S1. Linear potential sweep voltammetry plot with different deposition time of the (a) PED-CoPi-ZnO and (b) PD-CoPi-ZnO under under AM 1.5-irradiation in 0.2 M Na_2SO_4.

The overall photocurrent density was also increased by loading of CoPi onto ZnO NRAs, and the max photocurrent densities of 1.48 and 1.13 mA cm^{-2} at 1.23 V (vs. RHE) was generated by PED-CoPi(10)-ZnO NRAs and PD-CoPi10)-ZnO NRAs, respectively(Fig. S1). The steeper increase in photocurrent at potentials positive of the onset potential clearly illustrates the improved catalytic activity for water oxidation. The photocurrent density initially increased with CoPi deposition until a maximum current density is reached at ~10 min deposition time. The initial increase was ascribed to an increase in the number of active sites. However, beyond the optimal conditions, the ZnO NRAs surface may be blocked by the CoPi layer with limited access of electrolyte. According to the previous report[1], CoPi itself had no PEC water oxidation activity. Improved catalytic activity indicates that CoPi advantageous enhances the separation of the electron–hole pairs generated from ZnO NRAs and facilitates transfer the electron to the counter electrode to produce a larger photocurrent density.

Comparing with PED and PD, the PED of CoPi has a higher photocurrent. This is due to the PED with external bias lead to electron orientation of the migration, the valence band edge of two semiconductors located at a more positive potential than the oxidation potential of Co^{2+} ions and partly Co^{2+} ions to Co^{3+} ions to produce the CoPi co-catalysts on the ZnO surface[2]. The uniform CoPi film formed in the final and the full surface area participates in water oxidation, as desired.

The obvious onset potential can be found in PED-CoPi(10)-ZnO NRAs, which suggested a significant influence of surface recombination because this process is usually dominant at lower bias. With increasing bias, the surface effect weakens because pronounced band bending improves the charge separation, and bulk recombination becomes the main limiting factor[3]. In comparison with bare ZnO NRAs, -0.183 V (vs. Ag/AgCl), the photocurrent onset potential is cathodically shifted by ~ 0.119 V (vs. Ag/AgCl) for PED-CoPi(10) modified ZnO NRAs. which is attributed to the CoPi co-catalysts acting as a hole-trapping site tremendously mitigating hole–electron recombination and increase charge separation efficiency[4]. This trend illustrates the "kinetic bottleneck" effect described previously[5].

Furthermore, the top-down SEM image of PED and PD-CoPi-ZnO NRAs are displayed in Figure S2. PED-CoPi-ZnO NRAs reveals quantity of small irregular particles adhering to the hexagonal prisms and form the uniform patches intimate contact, which facilitate charge separation at the interface of CoPi and ZnO. As for PD-CoPi-ZnO NRAs, Figure S2 (b) reveals that CoPi agglomerations on the NRAs and conglutinate single nanorods together. Moreover, the EDS mapping characterizations demonstrated the homogenous distribution of Zn, O, Co and P in the as-prepared PED-CoPi(10)-ZnO NRAs.

In general, CoPi was finally chosen to be supported on the surface of the catalyst by PED.

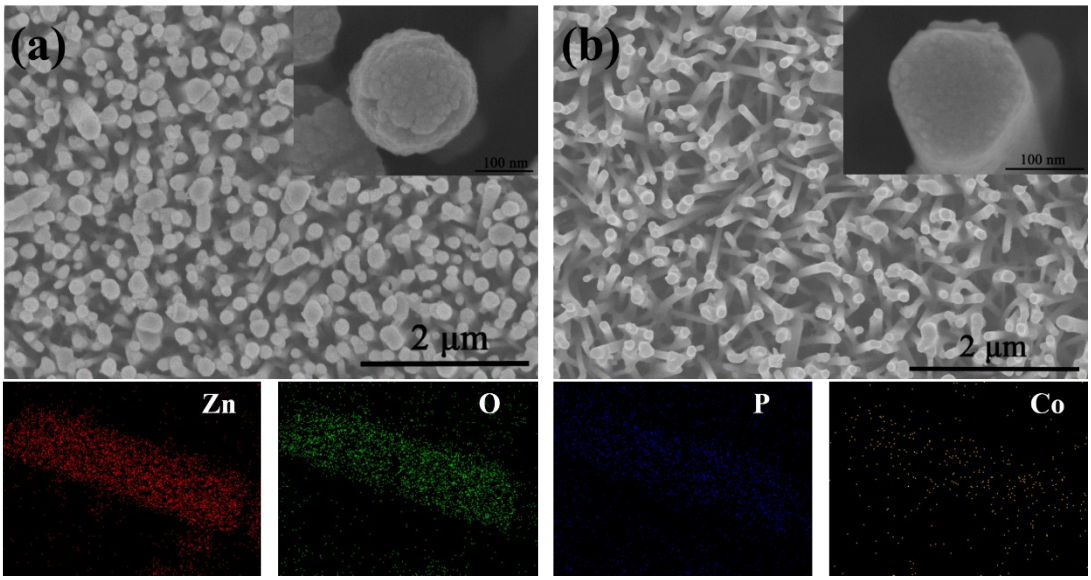

Fig. S2. Field-emission scanning electron microscope (FE-SEM) images of (a) PED-CoPi(10)-ZnO NRAs, (b) PD-CoPi-ZnO NRAs and (c) energy-dispersive X-ray spectrometer (EDS) elemental mapping images of the PED-CoPi(10)-ZnO NRAs.

PED-CoPi-ZnO NRAs reveals quantity of small irregular particles adhering to the hexagonal prisms and form the uniform patches intimate contact, which facilitate charge separation at the interface of CoPi and ZnO. As for PD-CoPi-ZnO NRAs, Figure S3(b) reveals that CoPi agglomerations on the nanorods and conglutinate single nanorods together. Moreover, the EDS mapping characterizations demonstrated the homogenous distribution of Zn, O, Co and P in the as-prepared PED-CoPi(10) -ZnO NRAs.

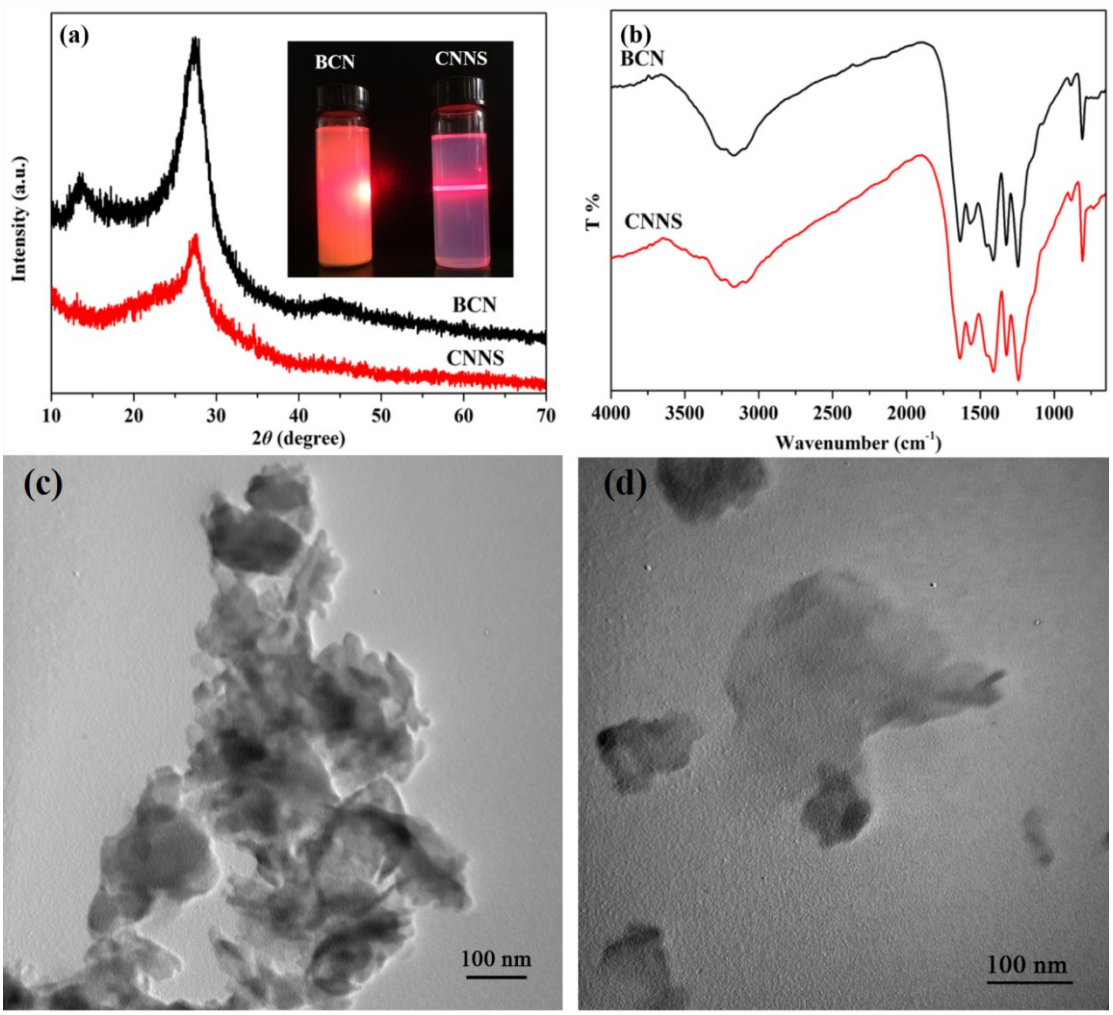

Fig. S3. (a) XRD patterns and (b) FTIR spectra of BCN and CNNS; TEM micrographs of (c) BCN and (e) CNNS.

For BCN, The peaks at 13.6° and 27.68° derived from the inplane repeated units of (100) reflection and the stacking of the conjugated aromatic systems in layered structure of (002) reflection, respectively[6]. Remarkably, for the CNNS, the intensities of these two peaks becomes less pronounced, which illustrated that the in-plane periodicity of the aromatic systems has been destroyed through the breakage of the hydrogen bonds by thermal oxidation etching and liquid exfoliation. The crystal structure of the nanosheets can be further confirmed by FTIR spectroscopy. Specifically, a series of peaks ranging from 1240 to 1640 cm^{-1} are ascribed to the stretching vibration mode of CN hetero-ring and the peak at 808 cm^{-1} can correspond to the ri-s-triazine units[7]. It was clear that the FTIR spectrum of CNNS was similar to that of BCN due to the same chemical structure.

Compared to BCN with a compact microstructure (Fig S3(c)), TEM images of CNNS shows well dispersion and laminar structure. That is, CNNS are successfully dispersed by thermal oxidation etching and solvent exfoliation method and the concentrations of CNNS could be tuned as required.

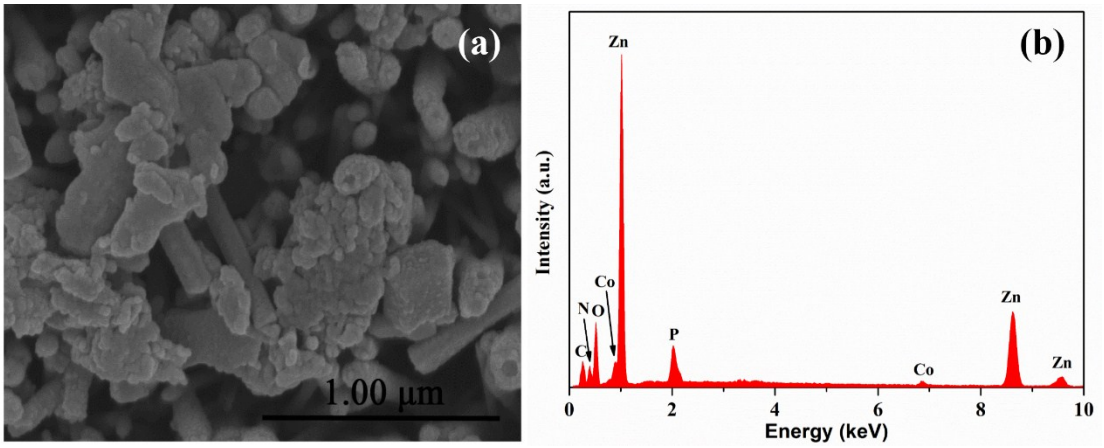

Fig.S4. (a) Field-emission scanning electron microscope (FE-SEM) images and (b) EDS data of CoPi(10)-CNNS(600)/ZnO NRAs.

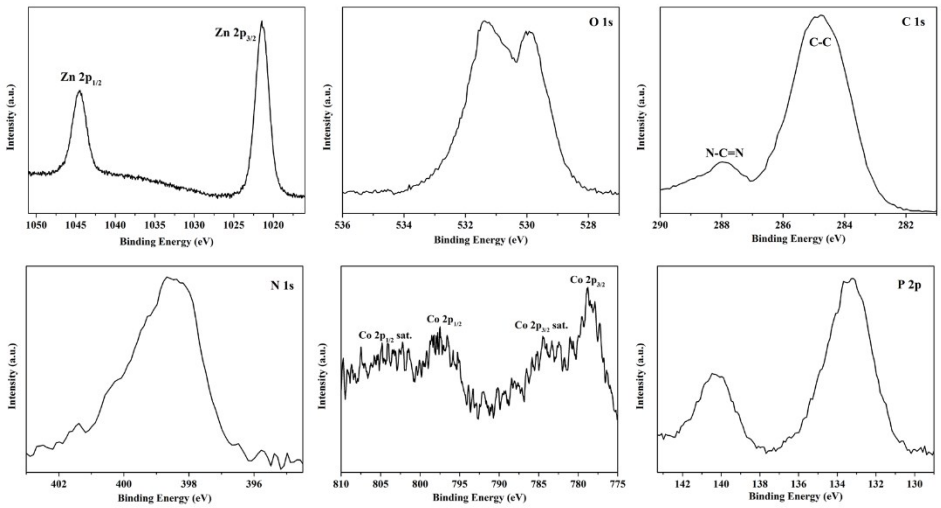

Fig.S5. XPS spectra of the CoPi-CNNS/ZnO NRAs photoanodes after photo-illumination with each elements.

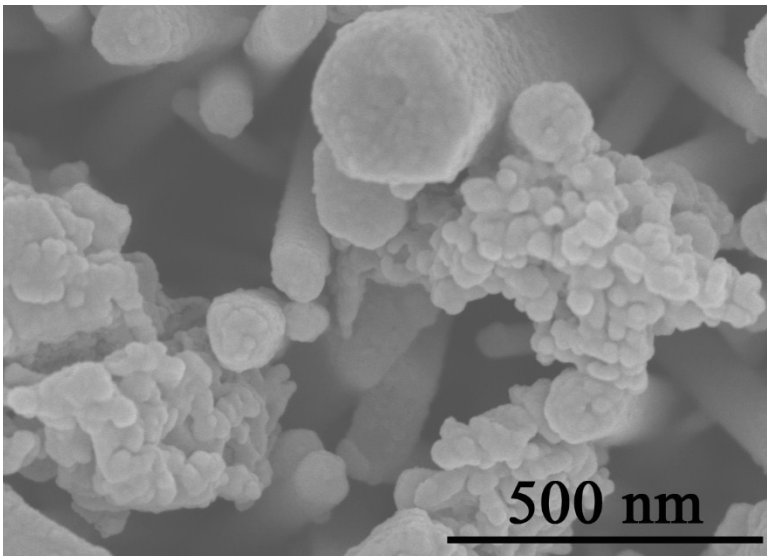

Fig.S6. Field-emission scanning electron microscope (FE-SEM) images of CoPi-CNNS/ZnO NRAs after photo-illumination.

References

1. T. H. Jeon, W. Choi and H. Park, Phys. Chem. Chem. Phys, 2011, **13**, 21392-21401.
2. E. M. Steinmiller and K. S. Choi, Proc. Natl. Acad. Sci. U. S. A, 2009, **106**, 20633-20636.
3. H. Gao, C. Liu, H. E. Jeong and P. Yang, *Acs Nano*, 2012, **6**, 234-240.
4. G. M. Carroll and D. R. Gamelin, *J. Mater. Chem. A*, 2015, **4**, 2986-2994.
5. D. R. Gamelin, G. M. Carroll and D. K. Zhong, *Energy Environ. Sci.* 2015, **8**, 577-584.
6. Q. Lin, L. Li, S. Liang, M. Liu, J. Bi and L. Wu, *Appl. Catal., B.* 2015, **163**, 135-142.
7. C. Liu, K. Wu, G. Meng, J. Wu, B. Peng, J. Hou, Z. Liu and X. Guo, *J. Mol. Catal. A: Chem.* 2017, **437**, 80-88.